A NEW METHOD OF PWM CONTROL FOR FORCED COMMUTATED CYCLOCONVERTERS USING MICROPROCESSORS

AKIO ISHIGURO, KATSUHISA INAGAKI, * MUNEAKI ISHIDA, SHIGERU OKUMA, YOSHIKI UCHIKAWA, ** KOJI IWATA

Department of Electronic Mechanical Engineering,
School of Engineering, Nagoya University
Furo-cho, Chikusa-ku, Nagoya 464, Japan
Tel. (052) 781-5111
* Department of Electrical Engineering,
School of Engineering, Mie University
1515 Kamihama-cho, Tsu 514, Japan
** Toyota College of Technology
Eisei-cho 2-1, Toyota 471, Japan

ABSTRACT — *In recent years PWM cycloconverters have been studied for eliminating dc links of conventional converter and inverter systems, and the various methods for generating PWM patterns have been proposed. A new real-time method for generating PWM patterns is proposed in this paper. The method realizes sinusoidal input and output currents, controllable input displacement factor regardless of load power factor, and maximum output voltage range. The proposed method is also effective to reduce higher and fractional harmonic components in the output voltages and the input currents, since the method uses three phases of the input voltage sources which are able to be connected to the output at the same time. Moreover, the higher harmonic oscillation in the input filters is reduced by changing the switching sequence of the PWM patterns adequately, and the distortion of the input current is improved. An output current feedback control based on the proposed switching pattern realizes an exact and quick response of the output current. Finally, feasibility of the proposed method is confirmed by simulations and experiments.*

INTRODUCTION

Forced commutated PWM cycloconverters have been studied for eliminating dc links of conventional rectifier and inverter systems. The PWM pattern generating method proposed by Ziogas et al. and Daniel et al. are based on the principle of the control for the PWM converters and PWM inverters.[1]~[6] Therefore, their methods allow only one or two phases of the input three phases to be connected to the output phases, and higher and fractional harmonic components are included in the output voltage and the input current waveforms. Furthermore, it is difficult to implement them so as to operate on real-time and with good waveforms.

A new real-time PWM pattern generating method is proposed in this paper, which realizes sinusoidal input and output current waveforms, controllable input displacement factor and maximum output voltage range. The proposed method is more advantageous to reduce higher and fractional harmonic components of the input and output waveforms than the previous methods, since it can make use of three phases of the input voltage sources at the same time.

The higher harmonic oscillation of the input filters is reduced by changing the switching sequence of the PWM patterns adequately, and the distortion of the input current is considerably improved.

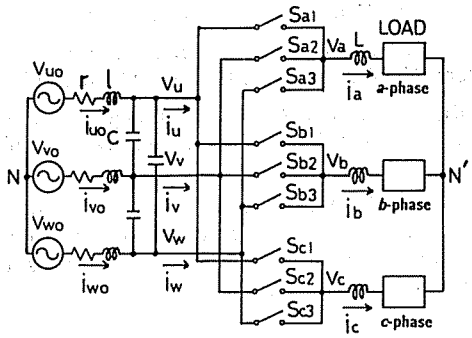

(a) Main circuit

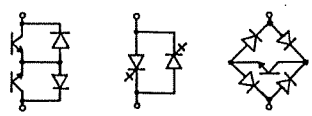

(b) Bidirectional switches

Fig. 1. PWM cycloconverter.

An output current feedback control based on the proposed switching pattern realizes an exact and quick response of the output current.

Simulations and experiments are carried out to confirm feasibility of the proposed methods.

CONTROL FUNCTION OF THE PWM CYCLOCONVERTER

Main Circuit of the PWM Cycloconverter

The main circuit of the PWM cycloconverter is shown in Fig.1(a) which consists of 9 self-turn-off bidirectional switches, input lCr filters, and symmetrical three phase loads. Examples of the switches are shown in Fig.1(b).

Input source voltages and input voltages which are outputs of lCr filters are as follows:

$$\begin{bmatrix} v_{uo} \\ v_{vo} \\ v_{wo} \end{bmatrix} = V_S \begin{bmatrix} cos\omega t \\ cos(\omega t - 2\pi/3) \\ cos(\omega t + 2\pi/3) \end{bmatrix} \quad (1)$$

$$\begin{bmatrix} v_u \\ v_v \\ v_w \end{bmatrix} = V \begin{bmatrix} cos(\omega t - \delta) \\ cos(\omega t - \delta - 2\pi/3) \\ cos(\omega t - \delta + 2\pi/3) \end{bmatrix} \quad (2)$$

88CH2565-0/88/0000-0712$01.00 © 1988 IEEE

where v_{uo}, v_{vo}, v_{wo} and v_u, v_v, v_w denote the input source voltages and the input voltages after the input lCr filters, respectively. V_S and V denote the magnitudes of the input source voltage and the input voltage after the input lCr filters, respectively. δ denotes the phase shift caused by the input lCr filters, and ω denotes the input angular frequency.

Control Requirements

(1) Frequency, amplitude, and phases of the output voltage can be controlled on real-time.
(2) Distortion of the input and output current waveforms is small.
(3) Input displacement factor can be controlled independently of load power factor. Input displacement factor of unity is realizable if needed.
(4) Magnitude of the output voltage range shall be maximized, satisfying the requirements (1)~(3).

The Principle of Frequency Conversion

Frequency conversion is regarded as a kind of coordinate transformation. Let's consider to transform a vector rotating clock-wise at an angular velocity ω (input angular frequency) on the stator axis ($\alpha - \beta$ coordinate system) to a vector rotating at an angular velocity ω_0 (output angular frequency). There are two principles which realize the transformation above-mentioned, one is *Principle 1* using $\alpha\ 1 - \beta\ 1$ axes rotating at a velocity of $\omega + \omega_0$, and the other is *Principle 2* using $\alpha\ 2 - \beta\ 2$ axes of $\omega - \omega_0$ as shown in Fig. 2.

Let's compare these two principles of transformation with the voltage and current vectors.

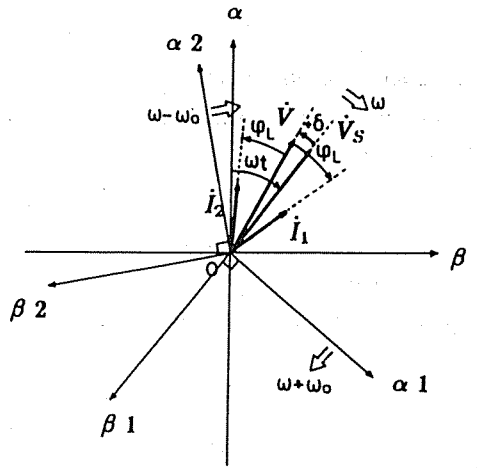

Fig. 2. Rotating coordinates of $\alpha\ 1 - \beta\ 1$, $\alpha\ 2 - \beta\ 2$ and voltage and current vectors.

(1) *Principle 1*

Voltage vector $\dot{V}$ rotates counter-clock-wise at a velocity of ω_0 viewed from $\alpha\ 1 - \beta\ 1$ axes rotating of $\omega + \omega_0$. When the load is inductive, output current vector $\dot{I}_1$ lags from the voltage vector $\dot{V}$ by φ_L. But viewed from $\alpha - \beta$ axes, $\dot{V}$ rotates clock-wise, and $\dot{I}_1$ leads to $\dot{V}$ by φ_L. Therefore, the input displacement factor is equal to the load power factor, but the signs of the reactive components of the input and the output currents are just opposite.

(2) *Principle 2*

$\dot{V}$ rotates clock-wise at a velocity of ω_0 viewed from $\alpha\ 2 - \beta\ 2$ axes of $\omega - \omega_0$. When the load is inductive, output current vector $\dot{I}_2$ lags from $\dot{V}$ by φ_L and also lags viewed from $\alpha - \beta$ axes. Therefore, the input real and reactive power do not change by the *Principle 2* transformation.

(3) *Proposed Control Principle — Composition of Principle 1 and Principle 2*

By using *Principle 1*, the difference of the phase angle between $\dot{I}_1$ and $\dot{V}_S$ becomes $-(\varphi_L - \delta)$, and by using *Principle 2*, the difference between $\dot{I}_2$ and $\dot{V}_S$ becomes $\varphi_L + \delta$. Therefore, by using the two principles, influence of the load reactive power to the input is able to be cancelled. For instance, the input displacement factor can be unity by using the two principles at the same ratio. The phase of input current vector $\dot{I}$ referred to $\dot{V}_S$ is determined by the initial phases of $\alpha\ 1 - \beta\ 1$ and $\alpha\ 2 - \beta\ 2$ axes referred to $\dot{V}_S$ as shown in Fig. 3 and Fig. 4. Fig. 3 shows the voltage vectors $\dot{V}_1$ and $\dot{V}_2$ transformed from the input voltage vector $\dot{V}$ by *Principle 1* and *Principle 2*, respectively. In Fig.4, φ_S is the phase of the axis of symmetry P with respect to $\alpha\ 1 - \beta\ 1$ and $\alpha\ 2 - \beta\ 2$ axes viewed from vector $\dot{V}_S$ and φ_C is the phase of $\alpha\ 1 - \beta\ 1$ and $\alpha\ 2 - \beta\ 2$ axes viewed from axis P at $t = 0$.

The voltage vectors $\dot{V}_1$ and $\dot{V}_2$ are mixed to make the output voltage vector $\dot{V}_L$, as shown in Fig.3. Therefore the phase of the output voltage can be controlled by φ_C. Fig.4 shows the current vectors $\dot{I}_{L1}$ and $\dot{I}_{L2}$ transformed from the output current vector $\dot{I}_L$ by *Principle 1* and *2*, respectively, which are mixed to make the input current vector $\dot{I}$. The phase of the vector $\dot{I}$ coincides with that of axis P, that is, φ_S. Therefore, the input displacement factor can be controlled by φ_S independently of the load power factor. The magnitude of the input current $\dot{I}$ is related to the load power factor. When $\varphi_S = 0$, the input displacement factor (after the input filters) can be kept unity.

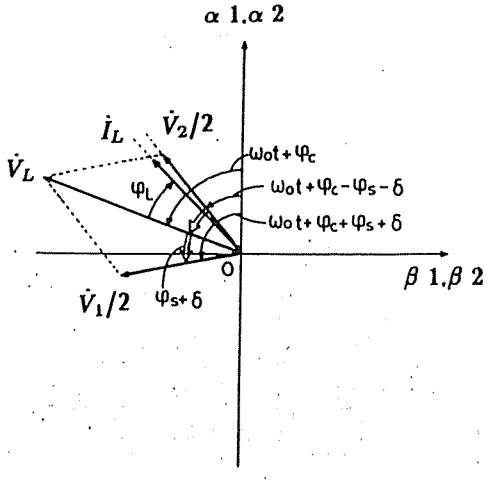

Fig. 3. Voltage vectors viewed from $\alpha\ 1 - \beta\ 1$ and $\alpha\ 2 - \beta\ 2$ coordinates, and composition of them, and output current vector.

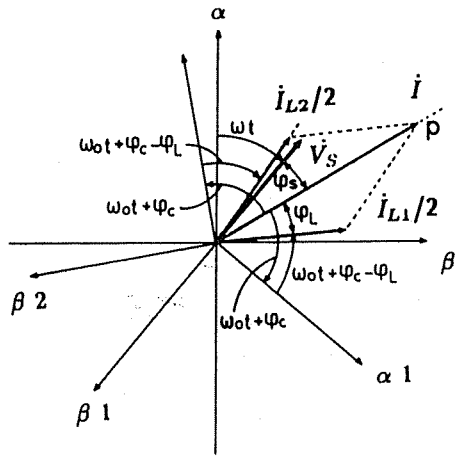

Fig. 4. Composition of input current vectors.

Formulation of Control Function

(1)*Definition of Control Function*

Since the input terminals are not allowed to be short-circuited and the output terminals are not allowed to be open-circuited, switches *Sa1~Sc3* are controlled on and off as in Fig.5. For real-time control, switching patterns are generated every sampling period T_S. Therefore, a control function is defined as a duty ratio within each T_S, and is denoted by $a_1 \sim c_3$, respectively. For instance, a_1 is defined by the following expression:

$$a_1 = (\text{on} - \text{time of } Sa1 \text{ during } T_S)/T_S \tag{3}$$

The following restrictions are obtained from Fig. 5:

$$\begin{aligned} a_1 + a_2 + a_3 &= 1 \\ b_1 + b_2 + b_3 &= 1 \\ c_1 + c_2 + c_3 &= 1 \end{aligned} \tag{4}$$

where

$$0 \leq a_n \leq 1,\ 0 \leq b_n \leq 1,\ 0 \leq c_n \leq 1,\ n = 1, 2, 3 \tag{5}$$

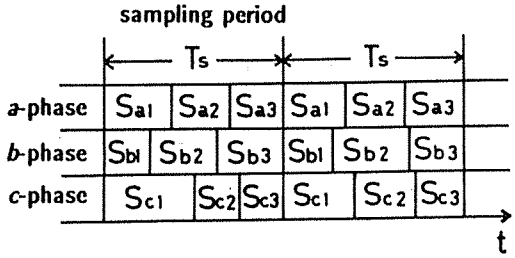

Fig. 5. Switching pattern.

The average values of the output voltages v_a, v_b, and v_c within T_S referred to the neutral point *N* are denoted by $\bar{v_a}, \bar{v_b}$, and $\bar{v_c}$, respectively. They are obtained from Fig.1(a) and Fig 5 as follows:

$$\begin{bmatrix} \bar{v_a} \\ \bar{v_b} \\ \bar{v_c} \end{bmatrix} = \begin{bmatrix} a_1 & a_2 & a_3 \\ b_1 & b_2 & b_3 \\ c_1 & c_2 & c_3 \end{bmatrix} \begin{bmatrix} v_u \\ v_v \\ v_w \end{bmatrix} \tag{6}$$

The currents $\bar{i_u}, \bar{i_v}$, and $\bar{i_w}$ which denote the average values of the input currents i_u, i_v, and i_w, respectively are also obtained as follows:

$$\begin{bmatrix} \bar{i_u} \\ \bar{i_v} \\ \bar{i_w} \end{bmatrix} = \begin{bmatrix} a_1 & b_1 & c_1 \\ a_2 & b_2 & c_2 \\ a_3 & b_3 & c_3 \end{bmatrix} \begin{bmatrix} i_a \\ i_b \\ i_c \end{bmatrix} \tag{7}$$

(2)*Control Function of the Principle 1*

The coordinate transformation of the *Principle 1* is expressed by the following control functions:

$$\begin{aligned} f_1 &= A\cos\{(\omega_0 + \omega)t + \varphi_C + \varphi_S\} \\ f_2 &= A\cos\{(\omega_0 + \omega)t + \varphi_C + \varphi_S - 2\pi/3\} \\ f_3 &= A\cos\{(\omega_0 + \omega)t + \varphi_C + \varphi_S + 2\pi/3\} \end{aligned} \tag{8}$$

$$\begin{bmatrix} a_1 & a_2 & a_3 \\ b_1 & b_2 & b_3 \\ c_1 & c_2 & c_3 \end{bmatrix} = \begin{bmatrix} f_1 & f_2 & f_3 \\ f_3 & f_1 & f_2 \\ f_2 & f_3 & f_1 \end{bmatrix} \equiv [F] \tag{9}$$

where A is the parameter of the voltage magnitude.

(3)*Control Function of the Principle 2*

The coordinate transformation of the *Principle 2* is expressed as follows:

$$\begin{aligned} g_1 &= A\cos\{(\omega_0 - \omega)t + \varphi_C - \varphi_S\} \\ g_2 &= A\cos\{(\omega_0 - \omega)t + \varphi_C - \varphi_S + 2\pi/3\} \\ g_3 &= A\cos\{(\omega_0 - \omega)t + \varphi_C - \varphi_S - 2\pi/3\} \end{aligned} \tag{10}$$

$$\begin{bmatrix} a_1 & a_2 & a_3 \\ b_1 & b_2 & b_3 \\ c_1 & c_2 & c_3 \end{bmatrix} = \begin{bmatrix} g_1 & g_2 & g_3 \\ g_2 & g_3 & g_1 \\ g_3 & g_1 & g_2 \end{bmatrix} \equiv [G] \tag{11}$$

(4)*Proposed Control Function*

We propose an arithmetic sum of the control functions of the *Principle 1 and 2*. The functions h_u, h_v, h_w are introduced to satisfy the restrictions in (4). The followings are the new control functions:

$$\begin{bmatrix} a_1 & a_2 & a_3 \\ b_1 & b_2 & b_3 \\ c_1 & c_2 & c_3 \end{bmatrix} = \frac{1}{2}[F] + \frac{1}{2}[G] + \begin{bmatrix} h_u & h_v & h_w \\ h_u & h_v & h_w \\ h_u & h_v & h_w \end{bmatrix} \tag{12}$$

The output voltages $\bar{v}_a, \bar{v}_b$, and $\bar{v}_c$ are obtained by substituting equations (2) and (12) into equation (6) as:

$$\begin{bmatrix} \bar{v_a} \\ \bar{v_b} \\ \bar{v_c} \end{bmatrix} = V_L \begin{bmatrix} cos(\omega_0 t + \varphi_C) \\ cos(\omega_0 t + \varphi_C + 2\pi/3) \\ cos(\omega_0 t + \varphi_C - 2\pi/3) \end{bmatrix}$$

$$+ \begin{bmatrix} h_u v_u + h_v v_v + h_w v_w \\ h_u v_u + h_v v_v + h_w v_w \\ h_u v_u + h_v v_v + h_w v_w \end{bmatrix} \quad (13)$$

where

$$V_L = \frac{3}{2} AV cos(\varphi_S + \delta) \quad (14)$$

The first terms of equation (13) are the output voltages and the second terms are the zero phase voltage components obtained by h_u, h_v and h_w. Assuming that the output current waveforms are sinusoidal by the filter effect of the load, the output currents are expressed as follows:

$$\begin{bmatrix} i_a \\ i_b \\ i_c \end{bmatrix} = I_L \begin{bmatrix} cos(\omega_0 t + \varphi_C + \varphi_L) \\ cos(\omega_0 t + \varphi_C + \varphi_L + 2\pi/3) \\ cos(\omega_0 t + \varphi_C + \varphi_L - 2\pi/3) \end{bmatrix} \quad (15)$$

The input currents $\bar{i}_u, \bar{i}_v, \bar{i}_w$ are obtained by substituting equations (12) and (15) into equation (7) as:

$$\begin{bmatrix} \bar{i_u} \\ \bar{i_v} \\ \bar{i_w} \end{bmatrix} = I \begin{bmatrix} cos(\omega t + \varphi_S) \\ cos(\omega t + \varphi_S - 2\pi/3) \\ cos(\omega t + \varphi_S + 2\pi/3) \end{bmatrix} \quad (16)$$

where

$$I = \frac{3}{2} AI_L cos(\varphi_C - \varphi_o) \quad (17)$$

Derivation of h_u, h_v, h_w and the Maximum Output Voltage

Consider the following variables:

$$\begin{aligned} X_1 &= cos(\omega t + \varphi_S) \\ X_2 &= cos(\omega t + \varphi_S - 2\pi/3) \\ X_3 &= cos(\omega t + \varphi_S + 2\pi/3) \end{aligned} \quad (18)$$

$$\begin{aligned} Y_1 &= cos(\omega_0 t + \varphi_C) \\ Y_2 &= cos(\omega_0 t + \varphi_C + 2\pi/3) \\ Y_3 &= cos(\omega_0 t + \varphi_C - 2\pi/3) \end{aligned} \quad (19)$$

Equations (18) and (19) express the required phases of the input currents and those of the output voltages, respectively. Equation (12) is expressed using equations (18) and (19) as:

$$\begin{bmatrix} a_1 & a_2 & a_3 \\ b_1 & b_2 & b_3 \\ c_1 & c_2 & c_3 \end{bmatrix} = A \begin{bmatrix} X_1Y_1 & X_2Y_1 & X_3Y_1 \\ X_1Y_2 & X_2Y_2 & X_3Y_2 \\ X_1Y_3 & X_2Y_3 & X_3Y_3 \end{bmatrix}$$

$$+ \begin{bmatrix} h_u & h_v & h_w \\ h_u & h_v & h_w \\ h_u & h_v & h_w \end{bmatrix} \quad (20)$$

The functions h_u, h_v and h_w have the following constraints from equations (5) and (20):

when $X_1 \geq 0$,

$$-AX_{1min}Y_n \leq h_u \leq 1 - AX_{1max}Y_n$$

when $X_1 < 0$,

$$-AX_{1max}Y_n \leq h_u \leq 1 - AX_{1min}Y_n$$

when $X_2 \geq 0$,

$$-AX_{2min}Y_n \leq h_v \leq 1 - AX_{2max}Y_n$$

when $X_2 < 0$,

$$-AX_{2max}Y_n \leq h_v \leq 1 - AX_{2min}Y_n$$

when $X_3 \geq 0$,

$$-AX_{3min}Y_n \leq h_w \leq 1 - AX_{3max}Y_n$$

Table 1. An example of h_u, h_v, h_w.

Switching mode	1	2	3	4	5	6
X1	+	+	−	−	−	+
X2	−	+	+	+	−	−
X3	−	−	−	+	+	+
h u	1-X1·maxYn	-X1·minYn	-X1·maxYn	1-X1·minYn	-X1·maxYn	-X1·minYn
h v	-X2·maxYn	-X2·minYn	1-X2·maxYn	-X2·minYn	-X2·maxYn	1-X2·minYn
h w	-X3·maxYn	1-X3·minYn	-X3·maxYn	-X3·minYn	1-X3·maxYn	-X3·minYn

when $X_3<0$,

$$-AX_{3max}Y_n \leq h_w \leq 1 - AX_{3min}Y_n \tag{21}$$

where ${}_{max}Y_n$ and ${}_{min}Y_n$ denote the maximum value and the minimum value of Y_1, Y_2, Y_3 at time t, respectively.

Equation (22) is derived from equations (4) and (20).

$$h_u + h_v + h_w = 1 \tag{22}$$

Functions h_u, h_v, h_w are listed on Table1. The functions are decided under the conditions that no switching occurs in a certain phase of *a, b, c*-phases within a period of T_S to reduce switching frequency and that equations (21) and (22) are satisfied. From equations (21) and (22), variable range of A is obtained as follows:

$$0 \leq a \leq 1/\sqrt{3} \tag{23}$$

The maximum amplitude of the output voltage is $A=1/\sqrt{3}$. When the input displacement factor is unity (*i.e.* $\varphi_S = 0$) and the phase shift by the input filters is negligible ($cos\delta \cong 1$), the maximum input-to-output voltage ratio is $\sqrt{3}/2$.

Effects of the Input lCr Filters

It is important to consider the effects of the input lCr filters on the control of the output voltage and the input displacement factor. The filter inductance l and the resistance r cause the phase shift δ of the input voltage and the capacitor C leads the input current. The input currents $\bar{i}_u, \bar{i}_v, \bar{i}_w$ have a phase shift of φ_S with respect to the source voltage $\dot{V}_S$ and $\varphi_S + \delta$ to the voltage after the lCr filters $\dot{V}$. For simplicity, the resistance r is neglected. Then we obtain:

$$\dot{V}_S = j\omega l(\dot{I} + j3\omega C\dot{V}) + \dot{V} \tag{24}$$

From equation (24)

$$\dot{V} = \dot{V}'_S - j\omega l\dot{I}/(1 - 3\omega^2 lC) \tag{25}$$

where

$$\dot{V}'_S = \dot{V}_S/(1 - 3\omega^2 lC) \tag{26}$$

is obtained.

These relations are described by a phasor diagram as shown in Fig.6, where the second term of equation (25) is the vector $\vec{BA'}$ vertical to the input current vector $\dot{I}$. Fig.7 shows a phasor diagram in the case of φ_S=0. From the phasor diagram, it is found that the capacitor current vector $\dot{I}_C$ is constant and that the phase of the input current vector $\dot{I}$ is constant at φ_S, even if the output current is changed. Moreover, the following equation is satisfied:

$$\dot{V}_L = \dot{V}cos(\varphi_S + \delta) = \dot{V}'_S cos\varphi_S \tag{27}$$

which indicates the output voltage $\dot{V}_L$ is determined by the input source voltage $\dot{V}_S$ and the phase demand φ_S of the input current $\dot{I}$, independently of the input voltage $\dot{V}$.

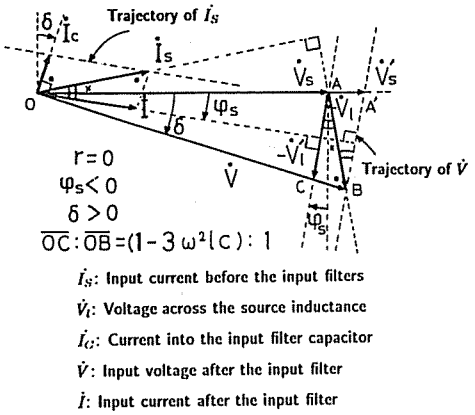

Fig. 6. Voltage and current vectors at the input and output of the input filters (in the case of $\varphi_S \neq 0$).

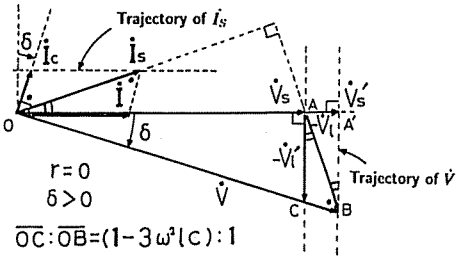

Fig. 7. Voltage and current vectors at the input and the output sides of the input filters (in the case of φ=0).

GENERATION METHOD OF SWITCHING FUNCTIONS

The control function mentioned in the previous chapter merely gives the duty ratio. More must be considered to generate the switching functions because the harmonic currents flow through the oscillatory input filters of the main circuit.

Making Switching Patterns from the Control Function

The switching patterns are generated by a single-edged modulation method, in which the control functions are sampled and held to be compared with a saw tooth wave during each sampling period T_S, as an example shown in Fig.8. The figure is the case that the control functions a_1 and $a_1 + a_2$ are sampled and held and hence the switching sequence becomes ***Sa1→Sa2→Sa3*** (denoted by 1→2→3).

As the result, the ratio of on intervals of ***Sa1***,***Sa2*** and ***Sa3*** to the sampling period T_S is proportional to a_1, a_2 and a_3, respectively. The switching patterns for switches ***Sb1***, ***Sb2***, ***Sb3*** and ***Sc1***, ***Sc2*** and ***Sc3*** are given in the same way.

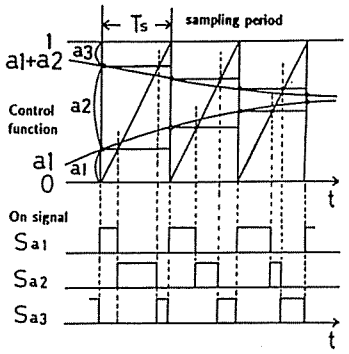

(switching sequence is order of 1→2→3.)

Fig. 8. Generation method of switching patterns.

Switching Sequence

A simple way to switch on *Sa1~Sc3* in a fixed sequence, for example 1→2→3, is called *Method 1*. But this method may cause a higher harmonic oscillation in the input filters because the input currents i_u, i_v, i_w change irregularly in an instant of changing the functions h_u, h_v, h_w as shown in Table 1.

The oscillation in the input filters can be suppressed and the input current waveforms are improved by changing the switching sequence so as to realize zero output voltage and zero input current at the beginning of the each sampling period as shown in Table 2. This method is called *Method 2*.

SYSTEM CONFIGURATION

Voltage Control System

Fig.9 shows the system configuration to realize the proposed output voltage control algorithm as mentioned in the previous chapter.

This system can make the input-to-output voltage ratio a little more than $\sqrt{3}/2$, which is the ratio in the case of sinusoidal output, if small distortion of the output voltages is permitted. This is realized by limiting the control functions $a_1 \sim c_3$ within the range of 0 to 1, and by making the waveforms of $AY_1 \sim AY_3$ rectangular asymptotically as the voltage demand becomes larger beyond the maximum sinusoidal output.

Operations surrounded by a broken-line in the figure are carried out using a microprocessor *MC68000*.

Table 2. Switching sequence of *Method 1* and *Method 2*.

Switching mode		1		2		3		4		5		6	
		1a	1b	2a	2b	3a	3b	4a	4b	5a	5b	6a	6b
max(X1, X2, X3)		X1		X2				X3					
min(X1, X2, X3)			X3			X1				X2			
Switch number with maximum absolute value of output voltage	Positive side	1		2				3				1	
	Negative side	2		3				1				2	
Phase in which the control function of the switch equals to unity		u−phase (maxYn)		w−phase (minYn)		v−phase (maxYn)		u−phase (minYn)		w−phase (maxYn)		v−phase (minYn)	
Switching state with zero vector (phases a,b,c)		(1 1 1)		(3 3 3)		(2 2 2)		(1 1 1)		(3 3 3)		(2 2 2)	
Switching Sequence	Method 1	1 2 3		1 2 3		1 2 3		1 2 3		1 2 3		1 2 3	
	Method 2	1 2 3		3 1 2		2 3 1		1 2 3		3 1 2		2 3 1	

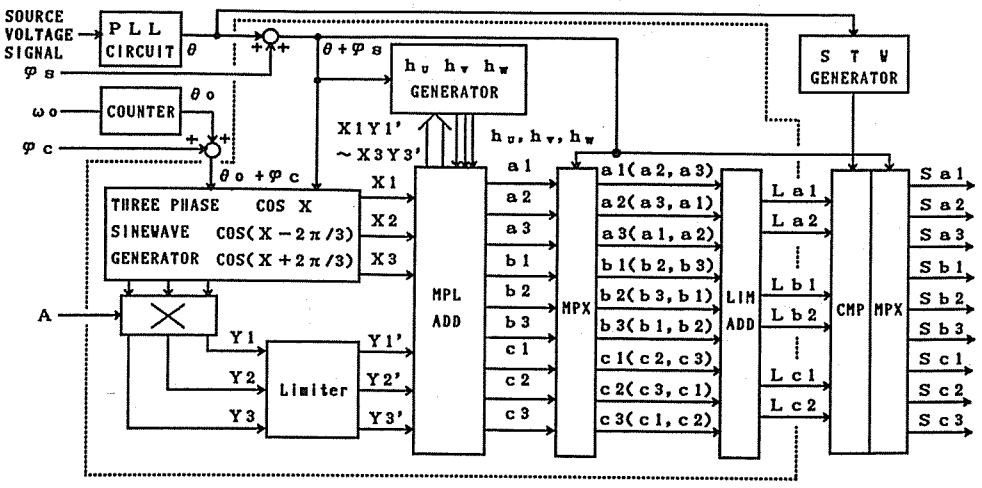

MPX : Multiplexer ADD : Adder
MPL : Multiplier CMP : Comparator
LIM : Limiter STW : Saw tooth wave

Fig. 9. System configuration.

Output Current Control System

The system configuration of the output current control is shown in Fig.10. The detected three-phase output currents i_a, i_b, and i_c are transformed into two-phase currents i_α, i_β. Two-phase current demands $i_\alpha{}^*$ and $i_\beta{}^*$ are obtained from demands of angular frequency ω_0, phase φ_o and magnitude I_L of the output currents.

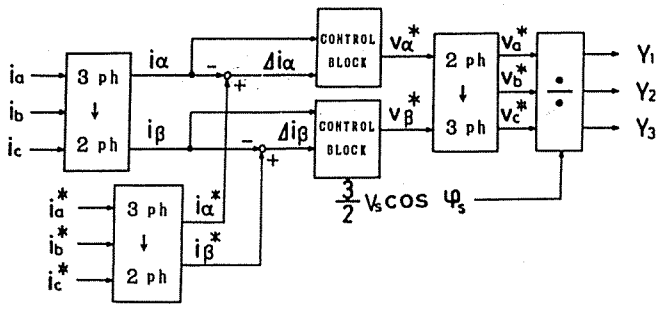

Fig. 10. Configuration of the output current control system.

From the current signals $i_\alpha, i_\beta, i_\alpha{}^*$ and $i_\beta{}^*$, the output voltage demands $v_\alpha{}^*$ and $v_\beta{}^*$ are calculated through the control blocks. Then $v_\alpha{}^*$ and $v_\beta{}^*$ are transformed into three-phase output voltage demands $v_a{}^*, v_b{}^*$ and $v_c{}^*$. Moreover, from equations (13) and (14), input variables AY_1, AY_2 and AY_3 for the voltage control system in Fig.9 are obtained by dividing $v_a{}^*, v_b{}^*$ and $v_c{}^*$ by $\dot{V}_S' cos\varphi_S$.

The control blocks are constructed as follows. Suppose that the load of each phase is a resistance R and a inductance L connected in series, the relationship between the output voltage vector $\dot{v}_o=(v_\alpha, v_\beta)$ and the output current vector $\dot{i}_o=(i_\alpha, i_\beta)$ is described by an equation (28):

$$\dot{v}_o = R\dot{i}_o + L\frac{d\dot{i}_o}{dt} \tag{28}$$

Proposed voltage control algorithm controls the average values of the output voltage over the sampling period T_S. Therefore, the output voltage vector $\dot{v}_o$ is approximated by the average value $\bar{v}_o$, which is regarded as sampled and held during T_S.

In this case, the sampled output current vector $\dot{i}_o(n+1)$ is given by

$$\dot{i}_o(n+1) = \dot{i}_o(n) + \{\frac{\bar{v}_o(n)}{R} - \dot{i}_o(n)\}\frac{R}{L}T_S \tag{29}$$

Making the current $\dot{i}_o(n+2)$ equal to the output current demand $\dot{i}_o^*(n)$, and adding PI controller to compensate the output voltage error caused by on-voltage drops of the switching devices, etc. the output voltage demand is given by:

$$\dot{v}_o^*(n+1) = \{\frac{L}{T_S} + K_P\}\Delta\dot{i}_o(n)$$

$$-\bar{v}_o(n) + 2\dot{i}_o(n)R + K_I\sum_{K=0}^{n}\Delta\dot{i}_o(k) \tag{30}$$

where K_P and K_I are proportional and integral gain, respectively, and $\Delta\dot{i}_o(n) = \dot{i}_o^*(n) - \dot{i}_o(n)$.

SIMULATION AND EXPERIMENTAL RESULTS

Output Voltage Control – Method 1

An example of patterns of the control functions $a_1 \sim c_3$ is shown in Fig.11. In this figure, the output voltage is maximized with $A=1/\sqrt{3}$ and $\varphi_S = 0$. Simulation and experimental results are shown in Fig.12,13 and Fig.14, with sampling time $T_S=260\mu s$, unity input displacement factor and the maximum output voltage. It is shown that the magnitude of the input source current depends on the load power factor. Fig.15 shows waveforms in the case of the input displacement angle of $-60°$. The conditions of simulations and experiments are described in each figure.

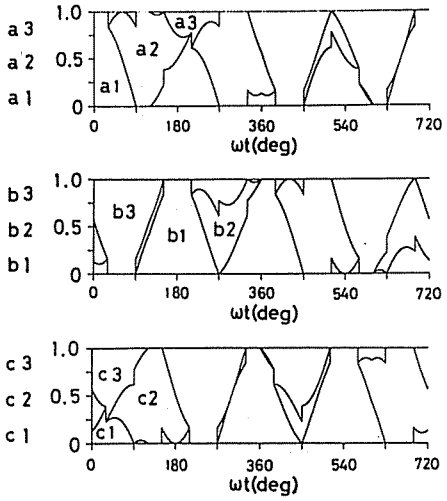

Fig. 11. Patterns of control functions $a_1 \sim c_3$.

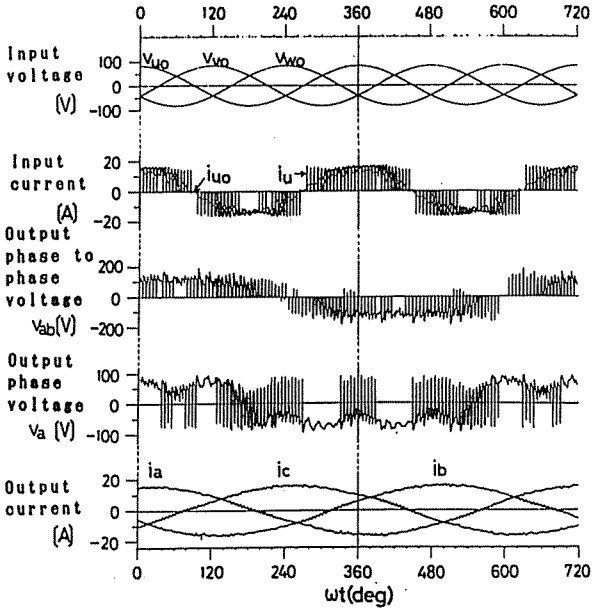

Fig. 12. Simulation results.

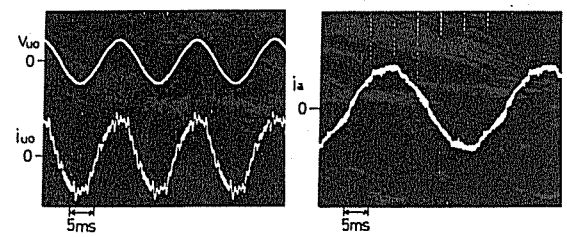

(i) Load power angle −4.7°

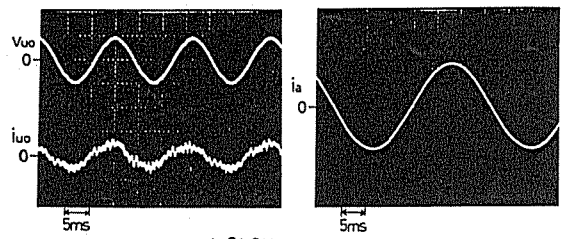

(ii) Load power angle −82°

Fig. 13. Current waveforms at the input and the output (input 60Hz, output 30Hz, φ_S=0).

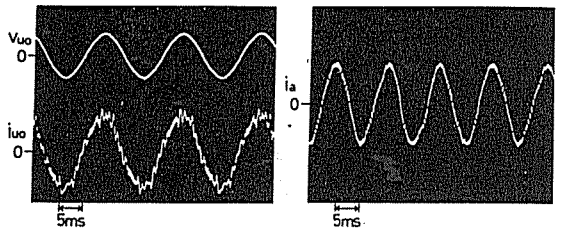

Fig. 14. Current waveforms at the input and the output (input 60Hz, output 90Hz, φ_S=0).

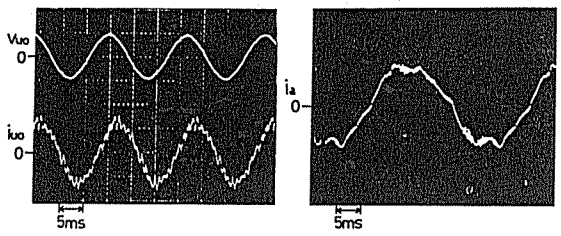

Fig. 15. Current waveforms at the input and the output (input 60Hz, output 30Hz, $\varphi_S = -60°$).

Effect of Changing Switching Sequence – Method 2

Figure.16 shows simulation results of *Method 1* and *Method 2*. The top figure shows the *u*-phase input source current i_{uo}, the *u*-phase input current after the input filter i_u, the input voltages after the input filters v_u, v_v, v_w and output currents i_a, i_b, i_c obtained from *Method 1*. The corresponding waveforms of *Method 2* are shown in the bottom figure. The simulation conditions are also described in the figure.

The input currents i_u, i_v, i_w, the input voltages v_u, v_v, v_w and the output currents i_a, i_b, i_c in Fig.16 are transformed into the trajectories of space vectors as shown in Fig.17 to confirm the improvement by *Method 2*. The left hand side shows the trajectories obtained by *Method 1*, and the right hand side shows the ones by *Method 2*. The top, middle and bottom figures show the trajectories of the input currents, the input voltages and the output currents, respectively.

By using *Method 2*, the vibrations of space vectors by higher harmonic components are approximately in steady state, that is, the width of the vibrations is approximately determined by the impedances of filter elements. On the other hand, *Method 1* causes the vibrations in the space vectors.

Figure.18 shows the experimental results of the *u*-phase input source current by *Method 1* and *Method 2*. The improvement of the input current i_{uo} by *Method 2* is confirmed.

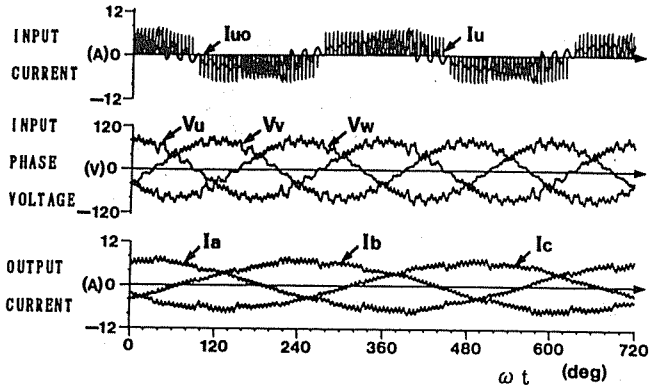

(a) *Method 1*

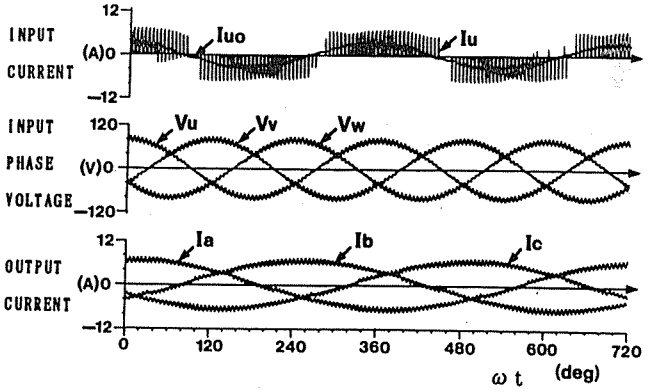

(b) *Method 2*

INPUT PHASE
TO PHASE VOLTAGE 100V, $\varphi s = 0$, $A = 1/\sqrt{3}$
INPUT 60Hz, r=0.5Ω, l=0.6mH, C=10μF
OUTPUT 30Hz, R=4Ω, L=3.6mH

Fig. 16. Simulation results of *Method 1* and *Method 2*.

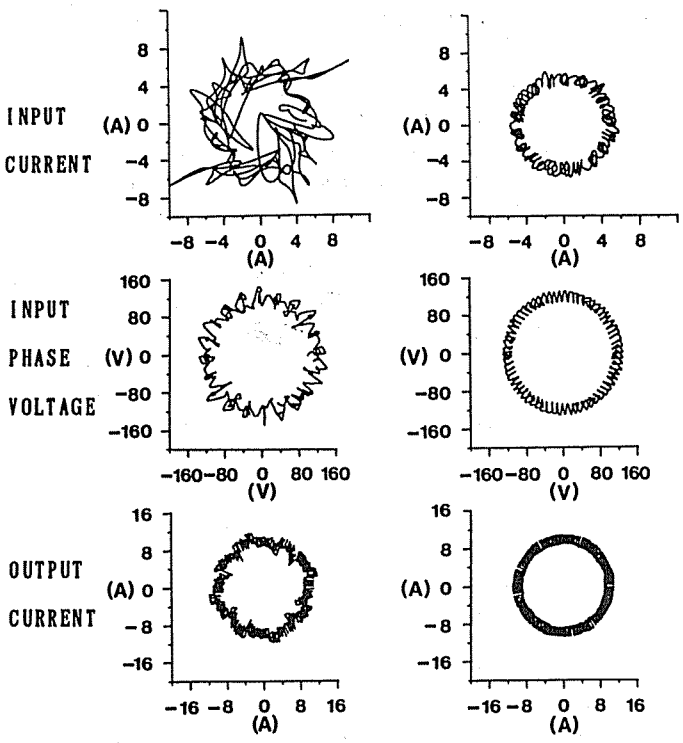

(a) *Method 1* (b) *Method 2*

Fig. 17. Simulation results of *Method 1* and *Method 2*.

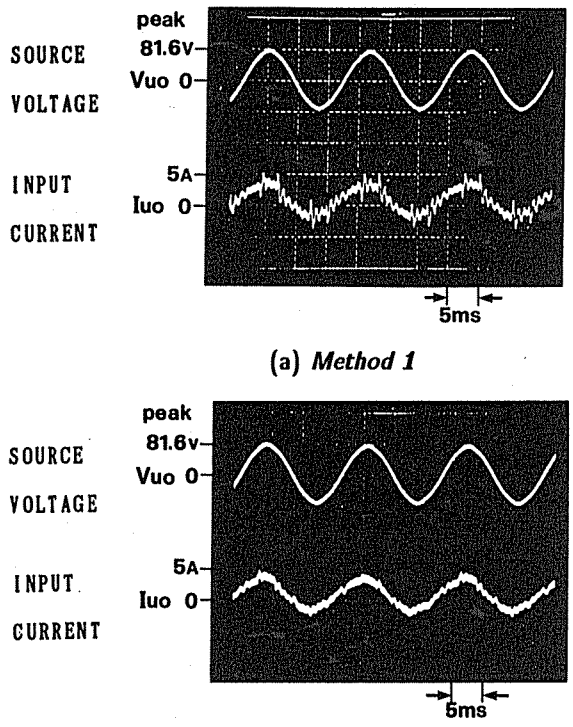

(a) *Method 1*

(b) *Method 2*

INPUT PHASE TO PHASE VOLTAGE 100V

INPUT 60Hz, r=0.5Ω, l=0.6mH, C=10μF

OUTPUT 30Hz, R=6Ω, L=3.5mH, A=1/√3, φs=0

Fig. 18. Experimental results of *Method 1* and *Method 2*.

Output Current Control

Figure.19, 20 and 21 show experimental results of the transient responses to changes of the demands of the amplitude of the output current, output frequency, and the output phase demands in the current control system shown in Fig.10, respectively. In this case, *Method 2* is used. Good dynamic responses are obtained.

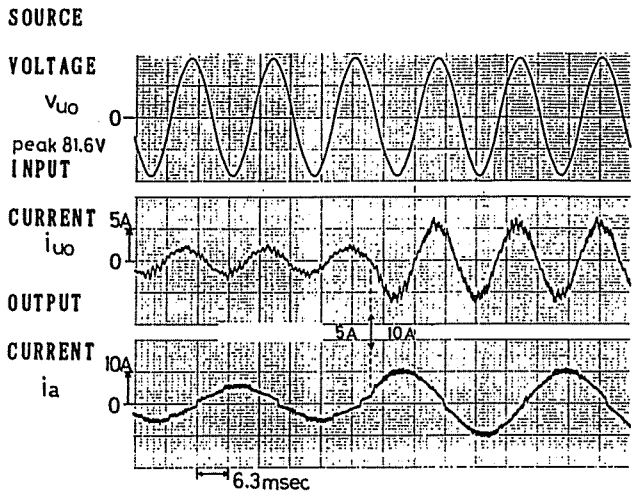

MAGNITUDE OF OUTPUT CURRENT 5A→10A

φs=0, l=0.6mH, c=10μF, L=3.5mH, R=4Ω

OUTPUT FREQUENCY 30Hz

Fig. 19. Waveforms of the input and output current (with change of magnitude).

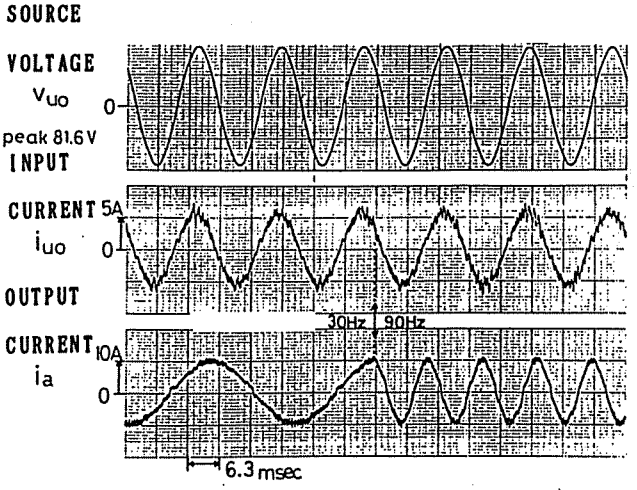

OUTPUT FREQUENCY 30Hz→90Hz

φs=0, l=0.6mH, c=10μF, L=3.5mH, R=4Ω

OUTPUT CURRENT 10A

Fig. 20. Waveforms of the input and output current (with change of output frequency).

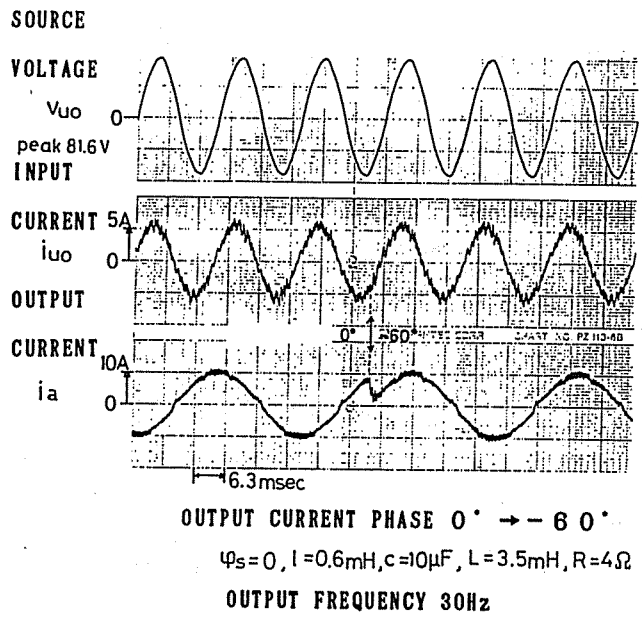

Fig. 21. Waveforms of the input and output current (with phase change).

CONCLUSIONS

The real-time output voltage and the output current control methods of the forced commutated PWM cycloconverters are studied in this paper. Results are as follows:

(1) The control algorithm is formulated by introducing the control functions derived from the principle of the frequency conversion.

(2) The proposed method realizes sinusoidal input and output currents, controllable input displacement factor independently of the load power factor, the maximum input-to-output voltage ratio $\sqrt{3}/2$.

(3) Higher harmonic oscillation in the input filters are reduced by changing the switching sequence of the PWM patterns adequately, and the distortion of the input source currents is improved.

(4) By using output current control based on output voltage control, exact and quick response of output current is realized.

(5) Feasibility of the proposed method is confirmed by simulations and experiments.

REFERENCES

[1] T. Ohnishi, et al., "A Novel PWM Technique for Three Phase Inverter/Converter," *IPEC-Tokyo, 384 (1983)*

[2] P.D. Ziogas, et al., "PWM Control Techniques for Rectifier Filter Minimization," *IEEE-Trans. Industr. Applic., IA-21, 1206 (1985)*

[3] P.D. Ziogas, et al., "Optimum System Design of a Three-Phase Rectifier-Inverter Type of Frequency Changer," *ibid., IA-21, 1215 (1985)*

[4] A.R. Daniel, et al., "Application of Power Transistors to Polyphase Regenerative Power Converters," *Proc. Instn Elect. Engrs, 125, 643 (1978)*

[5] P.D. Ziogas, et al., "Some Improved Forced Commutated Cycloconverter Structures," *IEEE-Trans. Industr. Applic. IA-21, 1242 (1985)*

[6] P.D. Ziogas, et al., "Analysis and Design of Forced Commuteated Cycloconverter Structures with Improved Transfer Characteristics," *IEEE PESC, 610 (1985)*